

Article

Thermoformable Conductive Compositions for Printed Electronics

Seyed Ismail Seyed Shahabadi ^{1,2}, Joel Ming Rui Tan ^{1,2} and Shlomo Magdassi ^{2,3,*} 

¹ School of Materials Science and Engineering, Nanyang Technological University, 50 Nanyang Avenue, Singapore 639798, Singapore

² Singapore-HUJ Alliance for Research and Enterprise (SHARE), The Smart Grippers for Soft Robotics (SGSR) Programme, Campus for Research Excellence and Technological Enterprise (CREATE), Singapore 138602, Singapore

³ Casali Center for Applied Chemistry, Institute of Chemistry, Edmond J. Safra Campus, The Hebrew University of Jerusalem, Jerusalem 91904, Israel

* Correspondence: magdassi@mail.huji.ac.il

Abstract: The development of three-dimensional printed electronics has garnered significant interest due to the ease of integration of electronic circuitry on 3D surfaces. However, it is still very challenging to achieve the desired conformability, stretchability, and adhesion of conductive pastes used for printing on thermoformable substrates. In this study, we propose the use of novel thermoformable ink composed of copper flakes coated with silver, which enables us to prevent the oxidation of copper, instead of the commonly used silver inks. Various polymer/solvent/flake systems were investigated, resulting in thermoformable conductive printing compositions that can be sintered under air. The best inks were screen printed on PC substrates and were thermoformed using molds with different degrees of strain. The effects of the various components on the thermoforming ability and the electrical properties and morphology of the resulting 3D structures were studied. The best inks resulted in a low sheet resistivity, 100 m Ω /□/mil and 500 m Ω /□/mil before and after thermoforming at 20%, respectively. The feasibility of using the best ink was demonstrated for the fabrication of a thermoformable 3D RFID antenna on PC substrates.

Keywords: printed electronics; thermoforming; copper conductive ink; screen printing



Citation: Shahabadi, S.I.S.; Tan, J.M.R.; Magdassi, S. Thermoformable Conductive Compositions for Printed Electronics. *Coatings* **2023**, *13*, 1548. <https://doi.org/10.3390/coatings13091548>

Academic Editor: Aomar Hadjadj

Received: 7 August 2023

Revised: 30 August 2023

Accepted: 31 August 2023

Published: 4 September 2023



Copyright: © 2023 by the authors. Licensee MDPI, Basel, Switzerland. This article is an open access article distributed under the terms and conditions of the Creative Commons Attribution (CC BY) license (<https://creativecommons.org/licenses/by/4.0/>).

1. Introduction

In recent years, increasing attempts have been made to develop the next generation of internet of things (IoT) components which, until recently, had limited integration into free-form 3D shapes due to the rigidity of their electronic circuitry resulting from their traditional manufacturing techniques. Nowadays, however, many researchers are advancing the manufacturing strategies for the fabrication of these components by developing deformable electronic circuits which can be divided into two main categories, i.e., rigid and flexible. While flexible circuits can be subjected to dynamic deformations such as elongation and compression and as such are based on elastomeric substrates, rigid circuits should retain their structure after their initial deformation from a 2D shape to their final 3D shape, and as such are based on rigid thermoplastic substrates [1,2].

Screen printing is a suitable printing method that can be used to produce both of the above-mentioned categories as it allows for the economical, high-volume production of printed electronics. The inks are generally based on polymer solutions that encapsulate the conductive particles. Printing is usually followed by sintering and, in the case of rigid free-form circuits, by a thermoforming process. Thermoforming is a simple, practical technique used extensively in packaging applications of pharmaceutical products, food containers, and medical equipment [3].

Among the different thermoforming methods, vacuum thermoforming is one of the most common variants. In this method, a 2D thermoplastic sheet is clamped in an airtight frame, then softened by heating through radiation or convection, drawn against a mold using a mechanical lever, and finally pressed against the mold using a vacuum. After cooling down, the component, which retains its final shape, is removed from the mold, and trimmed. The temperature range of this process depends on the substrate used but typically ranges between 120 and 200 °C. Due to its ease of use, thermoforming, along with other additive manufacturing methods, is gaining traction in producing free-form electronic component prototypes for control components in automotive and medical industries [4–6], antennas [7–13], sensors [14–17], diodes [18,19], solar cells [20], LED array [21] and epidermal electronics products [22–25].

Although thermoforming is widely used in its conventional form, the integration of printed electronics into this process is relatively recent. The effects of thermoforming on electrical performance and the limitations of printed electronics circuitry are not fully understood and process design guidelines are not fully developed.

There have been several studies on the fabrication of thermoformable printed electronics including the use of continuous laminated conductive foils, e.g., copper foil, sandwiched between thermoformable polymeric layers [10], printed traces on thermoformable substrates using 3D printers [26], as well as inks made from interconnected conductive particles such as graphene [27,28], Ag nanowire [29], Cu nanowire [30], and Ag flakes [31] bound by polymeric media. There are, however, fewer studies on screen-printed thermoformable circuits such as the study by Zulfiqar et al. [32] which investigated the effect of thermoforming strain, up to 12.5%, on the electrical performance of conductive inks. They prepared their ink using Ag powder and butyl carbitol and printed them on polycarbonate (PC) for components used in automotive lighting products and observed increases in resistance up to 633%. Wu et al. [13] used thermoforming to produce hemispherical coil antennas using commercial Ag paste from DuPont capable of a single-time stretch of up to 75%. Finally, Gong et al. [33] produced a regression model to describe the relationship between deformation, due to thermoforming, and electrical resistance of screen-printed traces using another commercial conductive Ag ink from DuPont. As can be seen, there are a few studies on screen-printed thermoformable circuits using conductive Ag flakes. Ag flakes are more affordable than gold and more air stable than copper. However, the price of Ag is still high, restricting its utility for many applications. One way to reduce the cost is to use Ag to coat copper flakes, resulting in flakes that are cheaper than Ag and more air stable than copper while remaining highly electrically conductive and more affordable. From an additive manufacturing viewpoint, producing thermoformable circuitry from these pastes is also much less time-consuming compared to the ones produced from etched copper electrodes. To the best of our knowledge, there is no study on the production of thermoformable circuits based on Ag-coated Cu flakes. In this study, we aim at preparing new thermoformable conductive pastes based on Ag-coated Cu flakes in polymeric solutions, for fabricating thermoformed coatings for application in printed electronics, focusing on plastic substrates.

2. Materials and Methods

2.1. Materials

All chemicals/materials purchased were used without additional processing. Poly-methyl methacrylate (PMMA, Sigma Merck 182230, Darmstadt, Germany), Polyvinyl butyral (PVB, Sigma Merck P110010), Poly (ethylene-vinyl acetate) (PEVA, Sigma Merck 340502), 1-phenoxy-2-propanol (PPh, Sigma Merck 484423), 2-phenoxyethanol (EPh, Sigma Merck 77699), Tri(ethylene glycol) dimethyl ether (TEDM, Sigma Merck T59803), Di(propylene glycol) methyl ether (DPM, Sigma Merck 484253), Tri(propylene glycol) methyl ether (TPM, Sigma Merck 484245), Di(ethylene glycol) monoethyl ether (DEE, Sigma Merck 537616), 2-(2-ethylhexyloxy) ethanol (EEH, Sigma Merck 476226), Di(ethylene glycol) hexyl ether (DEH, Sigma Merck 449393), and Di(propylene glycol) propyl ether (DPP, Sigma Merck

484210) were all purchased from Sigma Merck. Ag-coated Cu flakes were purchased from Guangzhou Hongwu Material Technology Co., Ltd. (Guangzhou, China), and polycarbonate (PC) film (LEXAN) was purchased from Sabic (Riyadh, Saudi Arabia).

2.2. Formulating Conductive Inks

Polymers were added to corresponding solvents at 60 °C and stirred for up to a few days to form resins containing 8 wt% polymers. These resins were mixed with Ag-coated Cu flakes at a ratio of 40:60 wt%, respectively, and the resulting composition was mixed in a planetary centrifugal mixer (THINKY ARE 310, Thinky USA, Laguna Hills, CA, USA) until homogenous ink was produced.

2.3. Sheet Resistivity Measurement

Inks were screen printed on PC using screens made with a polyester 47T mesh, stretched on a metal frame at a tension of 21–25 N with two emulsion thicknesses of 25 µm and 50 µm. After screen printing, PC films with wet prints were dried in an oven at 120 °C for 30 min. Sheet resistance ($m\Omega/\square$) was measured using a 4-point probe system (Jandel RM 3000, Jandel Engineering Limited, Leighton Buzzard, UK), and print thickness was measured using a digital gauge (Mitutoyo, Sakado, Japan) to calculate sheet resistivity ($m\Omega/\square/\text{mil}$).

2.4. Thermoforming

A tabletop vacuum thermoformer (Jintai) was used for thermoforming. Molds with nominal strains of 20, 60, and 100% were CNC milled from aluminum blocks. The nominal strains of the molds were calculated according to Equation (1). L and L_0 (1 cm) are shown in Figure 1. Molds were designed to allow stretching in one direction only. The resistance (R) of the prints was measured using a multimeter to calculate the resistance increase according to Equation (2). The normalized resistance increase is calculated according to Equation (3).

$$\text{Mould strain}(\%) = \frac{L - L_0}{L_0} \times 100 \quad (1)$$

$$R \text{ increase } (\%) = \frac{R \text{ after thermoforming} - R \text{ before thermoforming}}{R \text{ before thermoforming}} \times 100 \quad (2)$$

$$\text{Normalized } R \text{ increase } \left(\frac{\%}{\%} \right) = \frac{R \text{ increase}}{\text{Mould strain}} \quad (3)$$

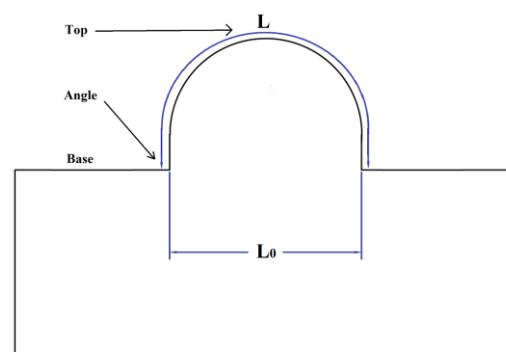


Figure 1. Typical cross-sectional view of a mold showing L_0 and L used to calculate the nominal strain of the molds. The three locations investigated by the light microscope and SEM are also designated.

2.5. Characterization

Scanning electron microscopy (SEM, Zeiss Supra 55, operated at 3 kV secondary electron, Zeiss, Jena, Germany) was used to characterize the surface morphology of the

films (Figure 1) at three locations, namely bottom, angle, and top, after thermoforming. Light microscopy (Olympus BX-51, Tokyo, Japan) was used to characterize the crack formation and their location.

Dynamic mechanical analysis was conducted on a Dynamic Mechanical Analyzer (DMA, TA instrument DMA850, New Castle, DE, USA). Samples were placed under a small load of 0.3 N, and the temperature was increased from 140 °C at a rate of 5 °C/min until sample failure to calculate the onset temperature for softening, which was used to find out the required time for the thermoforming process. By attaching a thermocouple to the film that is mounted on the thermoformer and recording the amount of time that is required to reach the softening temperature, we calculated the amount of time required for thermoforming.

3. Results and Discussion

The overall process of thermoforming is schematically presented in Figure 2. The pastes were screen printed on PC substrates and dried in an oven. Afterward, PC substrates were thermoformed using different molds, and the effects of polymer type and content, flake size and content, solvent, print patterns and thickness, and mold geometry on the electrical performance and morphology of the printed traces were studied.

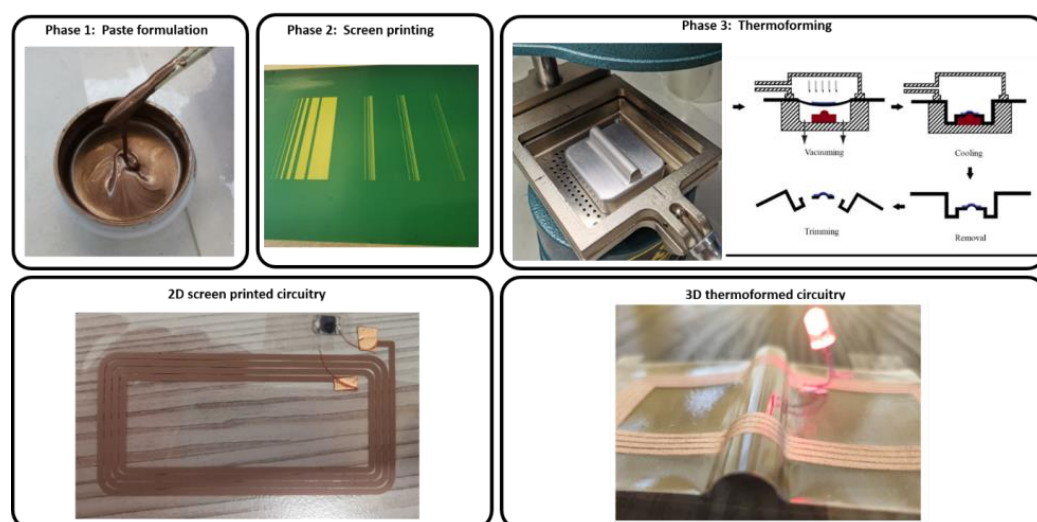


Figure 2. Schematic overview of the steps required to produce free-form 3D circuits. Phase 1. Polymer solution and Ag-coated Cu flakes are mixed. Phase 2. The resulting ink is screen printed on the substrate and the ink is dried in an oven. Phase 3. The substrate is clamped inside a thermoforming device, heated above softening, and conformed on a mold equipped with a vacuum pump. The resulting 3D polymer is then removed after cooling and trimmed. Image of 2D screen-printed RFID circuitry and 3D thermoformed circuitry.

3.1. Effect of Solvent on Sheet Resistivity

Conductive inks were made by mixing polymeric resin and copper flakes in a planetary mixer. Solutions with 8 wt% polymer content were mixed with flakes with an average size of 10 μm at a ratio of 40:60 wt%, respectively. The printed inks were cured in air, and the sheet resistivity was measured using a 4-point probe, and the thickness was measured by a profilometer.

In the first stage, a screening of solvents and polymers was performed. The results for PEVA-based Cu ink made from screening several solvents and shown in Figure 3 indicate that only the paste containing PEVA dissolved in PPh meets our sheet resistivity criterion (100 $\text{m}\Omega/\square/\text{mil}$). This finding signifies that even though solvents leave the paste after drying in the oven, they can still have substantial effects on the electrical properties of the pastes. PMMA was soluble in six of the solvents; however, pastes produced from

alkyl-based glycol ethers, i.e., alkoxy alcohols, namely TEDM, DPM, TPM, and DEE, did not have a good print due to transfer tailing during the separation of the screen from the substrate, i.e., splattering. After the identification of the solvent that enables good solubility of the polymer, and also good printability via screen printing, we evaluated the sheet resistivity for formulations with various polymers. In our research, the criterion for good electrical property was a sheet resistivity of $100 \text{ m}\Omega/\square/\text{mil}$ or below. The measurements showed that, in general, when the solvent with a phenyl ring was used, the resistivity was much lower ($\sim 100 \text{ m}\Omega/\square/\text{mil}$) as compared to that obtained while using aliphatic solvents (EEH, DP, DEH, and TPM), with a resistivity of $180\text{--}300 \text{ m}\Omega/\square/\text{mil}$. The solvent PPH is known for its coalescence ability for polymer-containing paints [34], and therefore, it can be assumed that the films formed in such formulations are more homogenous. That is why these three pastes were chosen for further investigation of their thermoformability.

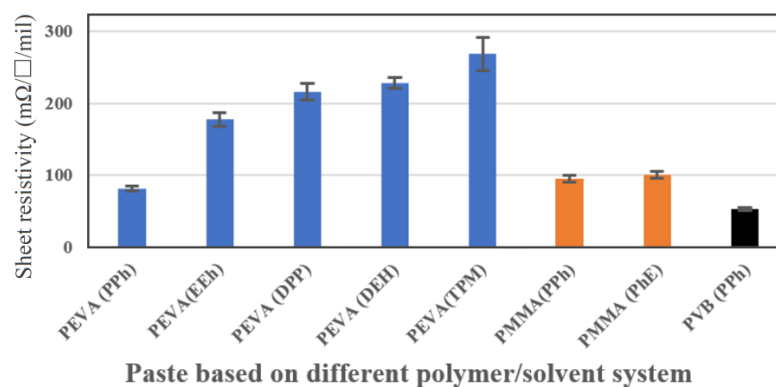


Figure 3. Sheet resistivity for pastes with identical formulations made from different polymer/solvent systems.

3.2. The Effects of Polymer and Solvent on Thermoformability

The DMA measurement of the substrate with the cured conductive ink (Figure 4) shows the variation in strain at different temperatures, suggesting $\sim 184^\circ\text{C}$ as the onset of softening temperature. Next, we fixed a thermocouple at the back of a PC film with the paste printed on top, clamped the film in our thermoforming device, and recorded the variation in temperature versus the time after we turned on the heating coil. The time it takes for the film to reach 200°C was recorded and applied for the thermoforming of the rest of the samples.

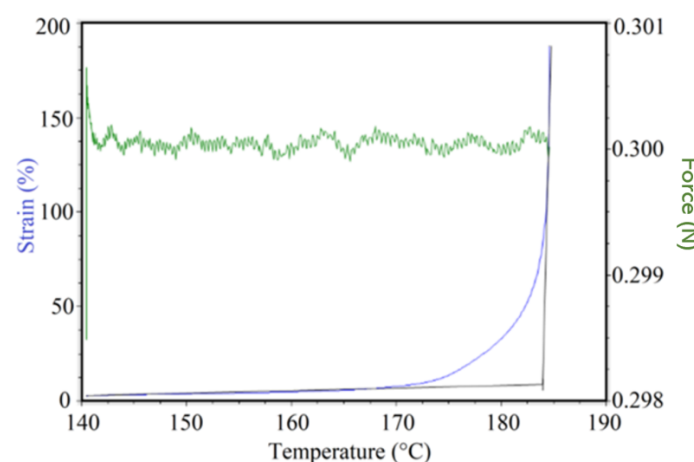


Figure 4. Variation in strain for PC film with printed paste on top at a constant load of 0.3 N versus temperature, showing $\sim 184^\circ\text{C}$ as the onset temperature for the softening of PC sheets with printed paste on top.

To study the effects of polymer binder on thermoformability, pastes based on PMMA, PVB, and PEVA solutions in PPh were screen printed on PC films, dried, and subjected to thermoforming using the 20% strain mold. The resistance of the traces was measured before and after thermoforming using a two-point probe. The calculated increase in the resistance of the films along with their pre-thermoforming values for resistance, as shown in Figure 5a, reveals the clear effect of polymer binder on the thermoformability of the pastes. We witnessed earlier that even though solvents leave the pastes after drying, they can have a profound effect on the sheet resistivity of the pastes. To discover if solvents have any effect on the electrical performance of the prints after thermoforming as well, identical PMMA pastes with different solvents, i.e., PPh and EPh, were produced, and the changes in their electrical performance after thermoforming were investigated. These pastes have similar sheet resistivity, but as follows from data in Figure 5b, the choice of solvent, even though it is not present during thermoforming, may have a noticeable effect on the resistance of the traces after thermoforming.

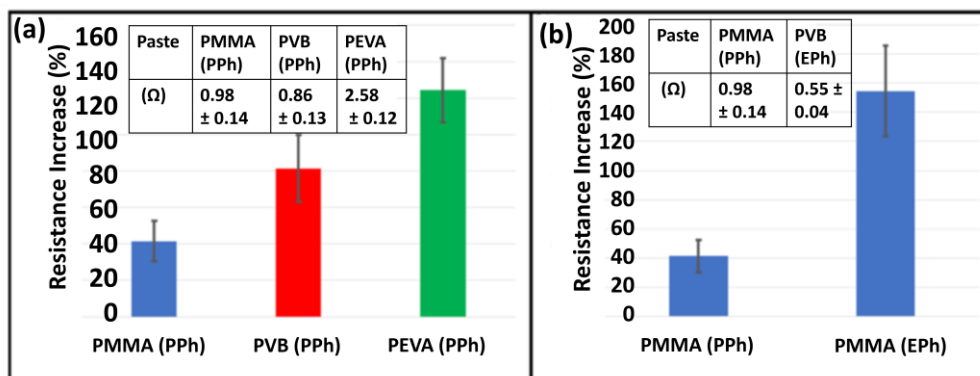


Figure 5. Resistance increase after thermoforming with the 20% strain mold for (a) identical pastes made from PMMA, PVB with PPh as solvent (b) identical pastes made from PMMA and two different solvents: PPh and EPh. The insets show average resistance values before thermoforming.

Several parameters may affect the change in resistivity after thermoforming: the morphology of the dried polymer film, the stretchability of the polymer film, and the melt-strength of the polymer. The T_g of the three tested polymers are PMMA~105 °C, PVB~80 °C, and PEVA~−38 °C [35]. Therefore, PVB and PEVA have a better ability to stretch and elongate than PMMA, resulting in larger distances between the copper particles during the thermoforming process, and eventually lower conductivity. Interestingly, the observed change in sheet resistivity (Figure 5) (PMMA < PVB < PEVA) is also in good agreement with the ranking of the T_g range (PMMA > PVB > PEVA) of the polymers.

3.3. The Effects of Mold Geometry and Print Thickness on Thermoformability

As seen in Figure 6, a paste made from PMMA(PPh) yielded the least resistance increase after thermoforming on the 20% strain mold; therefore, we further investigated the electrical performance of this paste after being thermoformed at even higher strains, i.e., 60% and 100%. In addition, we also investigated the effect of print thickness on the electrical performance of this formulation after thermoforming using two different screens with 25 and 50 μm emulsion sizes. The screen-printed traces were then dried in an oven and thermoformed using 20, 60, and 100% strain molds. The results of their resistance increase are shown in Figure 6a. As expected for both thicknesses, resistance increase goes up at higher strains. However, the rise in resistance increase is much less pronounced for the thicker print, i.e., 50 μm , and it plateaus at higher strains. This trend is more evident in Figure 6b, in which normalized values of the resistance increase are plotted. Normalized values are calculated by dividing the increase in resistance values by their corresponding strains, and they signify the proportion at which resistance increase values go up vis-a-vis strain increase. The figure clearly shows that the values of normalized resistance increase

go up with increasing strain for 25 μm prints, unlike the 50 μm prints, the values for which go down. We attribute this finding to the reinforcing effect of the paste printed on top of the substrate. Since these pastes are practically polymeric composites printed on top of PC substrates, they can increase the force required for conforming the films onto the molds as their thickness goes up. It should be noted that for samples with sharp angles of the thermoformed films, we observed that samples with 50 μm thickness do not fully conform to these sharp angles, and as such, the actual strain imposed on the traces is lower in the case of the 50 μm prints compared to the 25 μm ones, despite the nominal values being the same. This highlights that thicker prints have a higher resistance against deformation, hence causing the molding process to be less conforming.

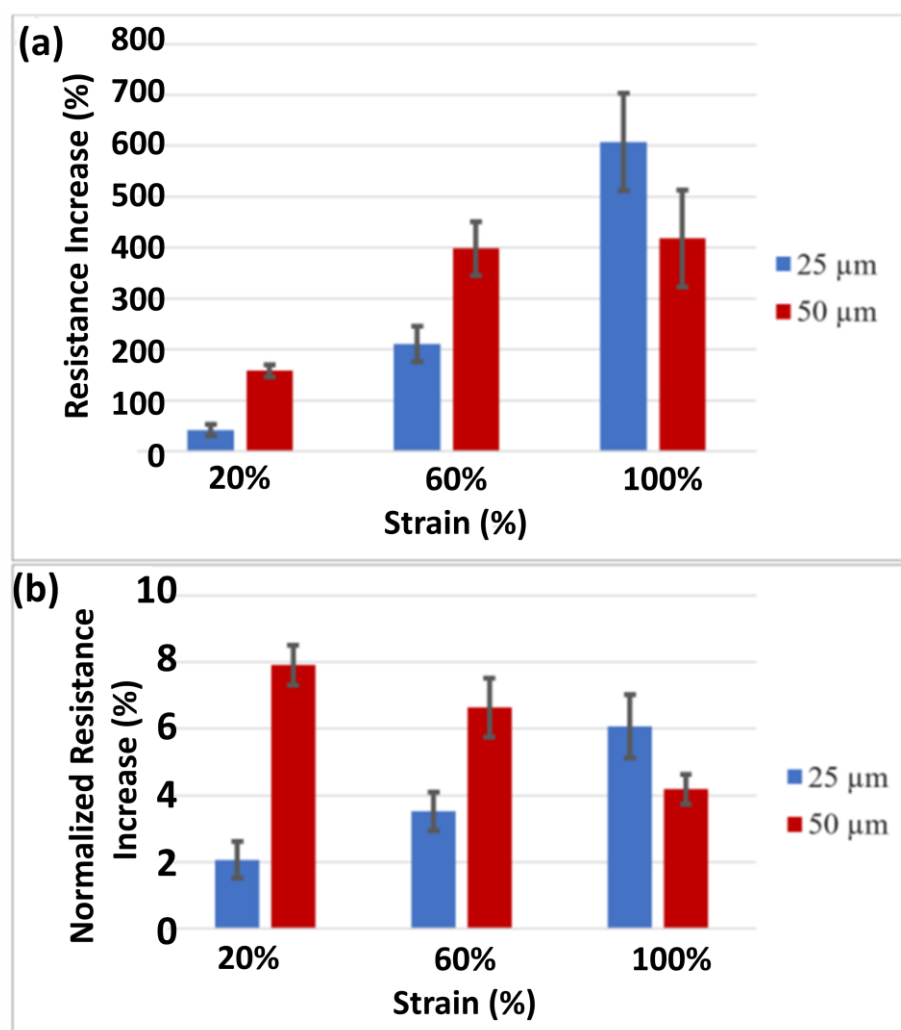


Figure 6. (a) Resistance increase and (b) normalized resistance increase for pastes made from PMMA(PPh) at different strains. The average resistance value for PMMA(PPh) films before thermoforming is 0.98 ± 0.14 .

3.4. Morphology of the Thermoformed Prints

The quality of printed conductive electrodes based on PMMA(PPh) printed using the 25 μm screen, and thermoformed on 20, 60, and 100% molds, was investigated via light microscopes and SEM (Figure 7). Since the original pastes were 3D, samples were first cut along the print lines, pulled from both ends and fixed between two glass slides for light microscopy imaging. For SEM, small pieces of the samples were cut and fixed on the stub. It was found that all films show a negligible change in the morphology of the samples at the base of the mold and the top of the mold. The most significant change

for all the samples can be observed where the samples conform to the sharp 90-degree angle of the molds. These changes are not as visible on the light microscope images for the 20 and 60% molds but noticeable for the 100% mold. SEM was employed to investigate the changes in the morphologies at smaller scales. SEM micrographs of the sample which was thermoformed on the base of the molds showed no noticeable cracks in this location for all samples. For the micrographs taken from the top of the mold, the samples prepared in the thermoforming mold of 20% strain did not show any cracks, which is not the case for the 60 and 100% molds, as these micrographs show the presence of sporadic microcracks for the 60% mold and slightly more cracks for the 100% mold. The most significant difference was seen for the micrographs taken from paste conformed to the sharp mold angle for all samples. For the 20% mold, these cracks seem to be narrow and shallow. The depth and width of the cracks increase for the 60% mold, and some of the cracks spread through the whole thickness of the film, making the substrate visible underneath. The most obvious change, as expected, occurred for the paste thermoformed on the sharp angle of the 100% mold, in which case, the cracks are even evident on the low-magnification micrograph. Here, a lot of cracks, many of them as deep as the thickness of the paste, can be observed, which are responsible for the drastic increase in the resistance of the films.

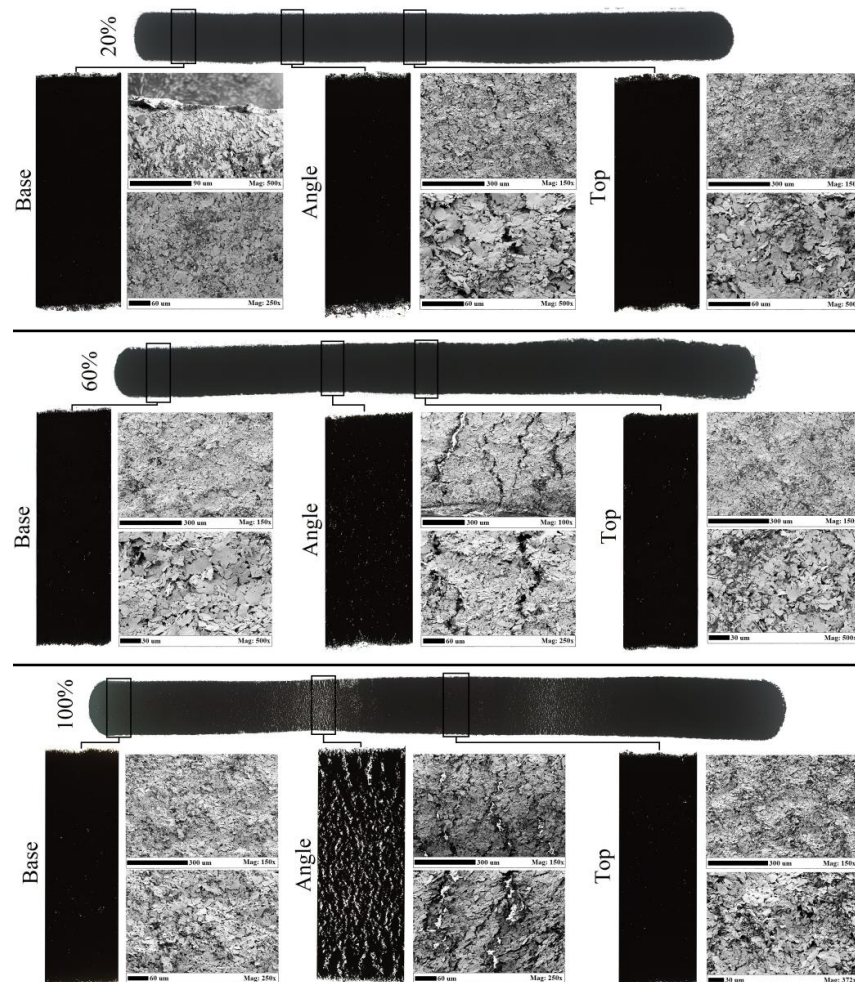


Figure 7. Low-magnification light microscope images for pastes molded on 20% strain mold (**top**), 60% strain mold (**middle**), and 100% strain mold (**bottom**). Higher-resolution light microscope images were taken from three locations for each sample: at the base of the mold, at the 90° angle, and at the top of the mold. SEM micrographs were taken from three locations as well, similar to high-magnification light microscope images.

3.5. Demonstration: Thermoformable RFID Circuit

Once we have established the printing compositions and the thermoforming process, we evaluated the feasibility of obtaining a functional thermoformed device. To demonstrate this, we used conductive inks composed of Ag-coated Cu flakes, with PMMA dissolved in PPh, to print an RFID antenna on PC substrates. After thermoforming (Figure 8) using the 60% mold, it was found that the continuity was not affected and an LED could still be lit, although the total resistance was increased from 11 ± 1 to 44 ± 8 ohm. In addition, it was found that the thermoformed antenna could be used for RFID communication, while the readability did not show any drop using a 13.56 MHz chip from a distance of 1 cm.

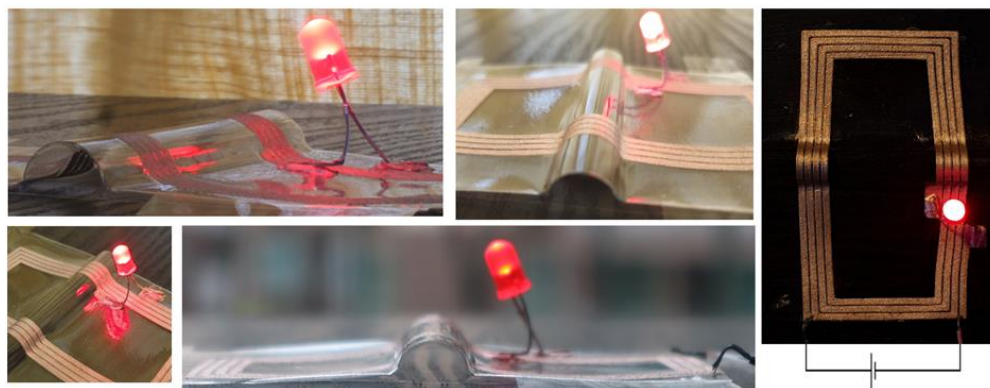


Figure 8. A typical RFID antenna design after printing on PC and thermoforming.

4. Conclusions

In this study, we explored different polymer/solvent/flake systems to obtain conductive printing compositions that are suitable for applications in plastic electronics which require thermoformability. Our results indicate that printing formulations composed of PMMA solutions in PPh with an 8 wt% polymer content and Ag-coated Cu flakes, in a 40:60 ratio, exhibited the best properties. The silver coating of the flakes prevents oxidation of the copper at the temperature experienced during the thermoforming process. These compositions, when screen printed on PC substrates, were analyzed for the effect of print thickness and mold geometry on their electrical properties. The best compositions experienced a sheet resistance increase of about four times only upon thermoforming using molds that induce strains of up to 20%. Morphological analysis of the films revealed a non-uniform strain distribution, with the highest strain observed at the mold's 90° angle. The PMMA-PPh-based printing ink was employed to print circuits for RFID antennas, and these antennas exhibited consistent RFID readability at a frequency of 13.56 MHz after thermoforming with strains up to 60%. These results suggest a potential approach to producing thermoformable plastic-printed electrical circuits, which are important for the emerging field of flexible hybrid electronics for applications in various fields including automotive, aerospace, and household electronics.

Author Contributions: Conceptualization, S.I.S.S., J.M.R.T. and S.M.; Investigation, S.I.S.S. and J.M.R.T. All authors have read and agreed to the published version of the manuscript.

Funding: This research is partially supported by a grant from the National Research Foundation, Prime Minister's Office, Singapore, under its Campus of Research Excellence and Technological Enterprise (CREATE) program (SGSR and NEW programs) and by AMat Singapore.

Institutional Review Board Statement: Not applicable.

Informed Consent Statement: Not applicable.

Data Availability Statement: Not applicable.

Conflicts of Interest: The authors declare no conflict of interest.

References

1. Kallmayer, C.; Schaller, F.; Loher, T.; Haberland, J.; Kayatz, F.; Schult, A. Optimized Thermoforming Process for Conformable Electronics. In Proceedings of the 2018 13th International Congress Molded Interconnect Devices (MID), Würzburg, Germany, 25–26 September 2018; pp. 1–6.
2. Rusanen, O.; Simula, T.; Niskala, P.; Lindholm, V.; Heikkinen, M. Injection Molded Structural Electronics Brings Surfaces to Life. In Proceedings of the 2019 22nd European Microelectronics and Packaging Conference & Exhibition (EMPC), Pisa, Italy, 16–19 September 2019; pp. 1–7.
3. Zhang, Y.; Chad Webb, R.; Luo, H.; Xue, Y.; Kurniawan, J.; Cho, N.H.; Krishnan, S.; Li, Y.; Huang, Y.; Rogers, J.A. Theoretical and Experimental Studies of Epidermal Heat Flux Sensors for Measurements of Core Body Temperature. *Adv. Healthc. Mater.* **2016**, *5*, 119–127. [[CrossRef](#)]
4. Balzereit, S.; Proes, F.; Altstädt, V.; Emmelmann, C. Properties of Copper Modified Polyamide 12-Powders and Their Potential for the Use as Laser Direct Structurable Electronic Circuit Carriers. *Addit. Manuf.* **2018**, *23*, 347–354. [[CrossRef](#)]
5. Fischer, A.J.; Meister, S.; Drummer, D. Effect of Fillers on the Metallization of Laser-Structured Polymer Parts. *J. Polym. Eng.* **2017**, *37*, 151–161. [[CrossRef](#)]
6. Jiménez, M.; Romero, L.; Domínguez, I.A.; del Espinosa, M.M.; Domínguez, M. Additive Manufacturing Technologies: An Overview about 3D Printing Methods and Future Prospects. *Complexity* **2019**, *2019*, 9656938. [[CrossRef](#)]
7. Adams, J.J.; Duoss, E.B.; Malkowski, T.F.; Motala, M.J.; Ahn, B.Y.; Nuzzo, R.G.; Bernhard, J.T.; Lewis, J.A. Conformal Printing of Electrically Small Antennas on Three-Dimensional Surfaces. *Adv. Mater.* **2011**, *23*, 1335–1340. [[CrossRef](#)] [[PubMed](#)]
8. Jobs, M.; Hjort, K.; Rydberg, A.; Wu, Z. A Tunable Spherical Cap Microfluidic Electrically Small Antenna. *Small* **2013**, *9*, 3230–3234. [[CrossRef](#)]
9. Yu, Y.; Liu, F.; Zhang, R.; Liu, J. Suspension 3D Printing of Liquid Metal into Self-Healing Hydrogel. *Adv. Mater. Technol.* **2017**, *2*, 1700173. [[CrossRef](#)]
10. Wu, K.; Zhou, Q.; Zou, H.; Leng, K.; Zeng, Y.; Wu, Z. High Precision Thermoforming 3D-Conformable Electronics with a Phase-Changing Adhesion Interlayer. *Micromachines* **2019**, *10*, 160. [[CrossRef](#)]
11. Tenchine, L.; Dassonville, O. Randomly Shaped 3D Electronics Using Innovative Combination of Standard Surface Mount Technologies and Polymer Processing. In Proceedings of the 2016 12th International Congress Molded Interconnect Devices (MID), Würzburg, Germany, 28–29 September 2016; pp. 1–6.
12. Chtioui, I.; Bossyut, F.; Bedoui, M.H. Finite Element Simulation of 2.5/3D Shaped and Rigid Electronic Circuits. In Proceedings of the 2016 13th International Conference on Computer Graphics, Imaging and Visualization (CGIV), Beni Mellal, Morocco, 29 March–1 April 2016; pp. 24–28.
13. Wu, Z.; Jobs, M.; Rydberg, A.; Hjort, K. Hemispherical Coil Electrically Small Antenna Made by Stretchable Conductors Printing and Plastic Thermoforming. *J. Micromech. Microeng.* **2015**, *25*, 027004. [[CrossRef](#)]
14. Tao, H.; Brenckle, M.A.; Yang, M.; Zhang, J.; Liu, M.; Siebert, S.M.; Averitt, R.D.; Mannoor, M.S.; McAlpine, M.C.; Rogers, J.A.; et al. Silk-Based Conformal, Adhesive, Edible Food Sensors. *Adv. Mater.* **2012**, *24*, 1067–1072. [[CrossRef](#)]
15. Yang, Y.; Vervust, T.; Dunphy, S.; Van Put, S.; Vandecasteele, B.; Dhaenens, K.; Degrendele, L.; Mader, L.; De Vriese, L.; Martens, T.; et al. 3D Multifunctional Composites Based on Large-Area Stretchable Circuit with Thermoforming Technology. *Adv. Electron. Mater.* **2018**, *4*, 1800071. [[CrossRef](#)]
16. Wimmer, A.; Reichel, H.; Schmidt, K. New Standards for 3D-Userinterfaces-Manufactured by a Film Insert Molding Process. In Proceedings of the 2018 13th International Congress Molded Interconnect Devices (MID), Würzburg, Germany, 25–26 September 2018; pp. 1–5.
17. Thomas, N.; Lähdesmäki, I.; Parviz, B.A. A Contact Lens with an Integrated Lactate Sensor. *Sens. Actuators B Chem.* **2012**, *162*, 128–134. [[CrossRef](#)]
18. Lee, C.-L.; Chang, K.-C.; Syu, C.-M. Silver Nanoplates as Inkjet Ink Particles for Metallization at a Low Baking Temperature of 100 °C. *Colloids Surfaces A Physicochem. Eng. Asp.* **2011**, *381*, 85–91. [[CrossRef](#)]
19. Park, J.H.; Seo, J.; Kim, C.; Joe, D.J.; Lee, H.E.; Im, T.H.; Seok, J.Y.; Jeong, C.K.; Ma, B.S.; Park, H.K.; et al. Flash-Induced Stretchable Cu Conductor via Multiscale-Interfacial Couplings. *Adv. Sci.* **2018**, *5*, 1801146. [[CrossRef](#)] [[PubMed](#)]
20. Yoon, J.; Li, L.; Semichaevsky, A.V.; Ryu, J.H.; Johnson, H.T.; Nuzzo, R.G.; Rogers, J.A. Flexible Concentrator Photovoltaics Based on Microscale Silicon Solar Cells Embedded in Luminescent Waveguides. *Nat. Commun.* **2011**, *2*, 343. [[CrossRef](#)] [[PubMed](#)]
21. Bhattacharya, R.; Wagner, S.; Yeh-Jiun, T.; Esler, J.R.; Hack, M. Organic LED Pixel Array on a Dome. *Proc. IEEE* **2005**, *93*, 1273–1280. [[CrossRef](#)]
22. Axisa, F.; Bossuyt, F.; Missine, J.; Verplancke, R.; Vervust, T.; Vanfleteren, J. Stretchable Engineering Technologies for the Development of Advanced Stretchable Polymeric Systems. In Proceedings of the PORTABLE-POLYTRONIC 2008—2nd IEEE International Interdisciplinary Conference on Portable Information Devices and the 2008 7th IEEE Conference on Polymers and Adhesives in Microelectronics and Photonics, Garmisch-Partenkirchen, Germany, 17–20 August 2008; pp. 1–8.
23. Huang, Z.; Hao, Y.; Li, Y.; Hu, H.; Wang, C.; Nomoto, A.; Pan, T.; Gu, Y.; Chen, Y.; Zhang, T.; et al. Three-Dimensional Integrated Stretchable Electronics. *Nat. Electron.* **2018**, *1*, 473–480. [[CrossRef](#)]
24. Kaltenbrunner, M.; Sekitani, T.; Reeder, J.; Yokota, T.; Kuribara, K.; Tokuhara, T.; Drack, M.; Schwödiauer, R.; Graz, I.; Bauer-Gogonea, S.; et al. An Ultra-Lightweight Design for Imperceptible Plastic Electronics. *Nature* **2013**, *499*, 458–463. [[CrossRef](#)]

25. Kim, D.-H.; Lu, N.; Ma, R.; Kim, Y.-S.; Kim, R.-H.; Wang, S.; Wu, J.; Won, S.M.; Tao, H.; Islam, A.; et al. Epidermal Electronics. *Science* **2011**, *333*, 838–843. [[CrossRef](#)]
26. Yan, Q.; Dong, H.; Su, J.; Han, J.; Song, B.; Wei, Q.; Shi, Y. A Review of 3D Printing Technology for Medical Applications. *Engineering* **2018**, *4*, 729–742. [[CrossRef](#)]
27. Ng, L.W.T.; Zhu, X.; Hu, G.; Macadam, N.; Um, D.; Wu, T.; Le Moal, F.; Jones, C.; Hasan, T. Conformal Printing of Graphene for Single- and Multilayered Devices onto Arbitrarily Shaped 3D Surfaces. *Adv. Funct. Mater.* **2019**, *29*, 1807933. [[CrossRef](#)]
28. Zhang, Y.; Gui, Y.; Meng, F.; Li, L.; Gao, C.; Zhu, H.; Hao, Y. Graphene Water Transfer Printing for 3D Surface. In Proceedings of the 2016 IEEE 29th International Conference on Micro Electro Mechanical Systems (MEMS), Shanghai, China, 24–28 January 2016; pp. 13–16.
29. Williams, N.X.; Noyce, S.; Cardenas, J.A.; Catenacci, M.; Wiley, B.J.; Franklin, A.D. Silver Nanowire Inks for Direct-Write Electronic Tattoo Applications. *Nanoscale* **2019**, *11*, 14294–14302. [[CrossRef](#)]
30. Ding, S.; Jiu, J.; Gao, Y.; Tian, Y.; Araki, T.; Sugahara, T.; Nagao, S.; Nogi, M.; Koga, H.; Suganuma, K.; et al. One-Step Fabrication of Stretchable Copper Nanowire Conductors by a Fast Photonic Sintering Technique and Its Application in Wearable Devices. *ACS Appl. Mater. Interfaces* **2016**, *8*, 6190–6199. [[CrossRef](#)]
31. Cui, H.-W.; Jiu, J.-T.; Sugahara, T.; Nagao, S.; Sugauma, K.; Uchida, H.; Kihara, K. Solidification and Thermal Degradation of Printable, Stretchable Electrical Conductor from Waterborne Polyurethane and Silver Flakes. *J. Therm. Anal. Calorim.* **2015**, *122*, 295–305. [[CrossRef](#)]
32. Zulfiqar, S.; Saad, A.A.; Sharif, M.F.M.; Samsudin, Z.; Ali, M.Y.T.; Ani, F.C.; Ahmad, Z.; Abdullah, M.K. Alternative Manufacturing Process of 3-Dimensional Interconnect Device Using Thermoforming Process. *Microelectron. Reliab.* **2021**, *127*, 114373. [[CrossRef](#)]
33. Gong, Y.; Cha, K.J.; Park, J.M. Deformation Characteristics and Resistance Distribution in Thermoforming of Printed Electrical Circuits for In-Mold Electronics Application. *Int. J. Adv. Manuf. Technol.* **2020**, *108*, 749–758. [[CrossRef](#)]
34. Yi, W.; Zhonghua, C.; Fei, Y. Coalescing Aid Influences on Acrylic Latexes Property and Film Formation Process. *Indian J. Mater. Sci.* **2016**, *2016*, 1380791. [[CrossRef](#)]
35. Mark, J.E. *Polymer Data Handbook*; Oxford University Press: Oxford, UK, 2009; ISBN 9780195181012.

Disclaimer/Publisher’s Note: The statements, opinions and data contained in all publications are solely those of the individual author(s) and contributor(s) and not of MDPI and/or the editor(s). MDPI and/or the editor(s) disclaim responsibility for any injury to people or property resulting from any ideas, methods, instructions or products referred to in the content.